Nonequilibrium dynamics of the complex Ginzburg-Landau equation: Numerical results in two and three dimensions

Subir K. Das and Sanjay Puri
School of Physical Sciences, Jawaharlal Nehru University, New Delhi 110067, India
(Received 14 December 2001; published 3 April 2002)

This paper is the second of a two-stage exposition, in which we study the nonequilibrium dynamics of the complex Ginzburg-Landau (CGL) equation. We use spiral defects to characterize the system evolution and morphologies. In the first paper of this exposition [S.K. Das, S. Puri, and M.C. Cross, Phys. Rev E **64**, 046206 (2001)], we presented analytical results for the correlation function of a single spiral defect, and its short-distance singular behavior. We had also examined the utility of the Gaussian auxiliary field ansatz for characterizing multispiral morphologies. In this paper, we present results from an extensive numerical study of nonequilibrium dynamics in the CGL equation with dimensionality $d=2,3$. We discuss the behavior of domain growth laws; real-space correlation functions; and momentum-space structure factors. We also compare numerical results for the correlation functions and structure factors with analytical results presented in our first paper.

DOI: 10.1103/PhysRevE.65.046123 PACS number(s): 64.60.Cn, 05.70.Ln

I. INTRODUCTION

The complex Ginzburg-Landau (CGL) equation has the general form

$$\frac{\partial \psi(\vec{r},t)}{\partial t} = \psi(\vec{r},t) + (1+i\alpha)\nabla^2\psi(\vec{r},t) - (1+i\beta)|\psi(\vec{r},t)|^2\psi(\vec{r},t), \quad (1)$$

where the complex order-parameter field $\psi(\vec{r},t)$ depends upon space $\vec{r}$ and time t and α, β are real parameters. The CGL equation constitutes the natural description of many physical systems (e.g., chemical oscillations [1], thermal convection in binary fluids [2], multimode lasers [3], etc.), and exhibits a wide range of dynamical behavior as the parameters α and β are varied. For an overview of applications of the CGL equation, the reader is referred to the paper by Cross and Hohenberg [4].

In the limit $\alpha,\beta\to\infty$, the CGL equation reduces to the nonlinear Schrödinger (NLS) equation, which has extensive applications in nonlinear optics and plasma physics. The NLS equation admits of soliton solutions and is solvable by means of the inverse-scattering transformation [5]. On the other hand, when $\alpha=\beta=0$, the CGL equation reduces to the dynamical XY model, which is not analytically tractable. There has been much recent interest in the phase ordering dynamics of the XY model (and analogous models), i.e., the nonequilibrium evolution of the disordered system, when it is rendered thermodynamically unstable by a rapid quench below the critical temperature [6,7]. Essentially, the ordering dynamics is driven by the annihilation of defects, e.g., vortices in the case of the XY model. These spatially extended defects provide a basis for characterizing statistical properties of the evolving morphology, e.g., time-dependent correlation functions and structure factors, domain growth laws, etc. [7].

Recently, we have initiated a study of phase ordering (nonequilibrium) dynamics in the CGL equation [8,9]. The appropriate defect structure that characterizes the evolving morphology in this case is the spiral, which is a generalization of the vortex defect in the XY model. In the first paper of this two-stage exposition [8], we have presented analytical results for the real-space correlation function and momentum-space structure factor corresponding to a single-spiral defect. In particular, we were interested in the short-distance singularity of the correlation function, and its implication for the large-wave-vector behavior of the structure factor. In our earlier papers [8,9], we also presented some numerical results from simulations of the $d=2$ CGL equation with $\alpha=0$. This paper is the second and final stage of our exposition. Here, we present comprehensive numerical results, obtained from simulations of phase ordering dynamics in the CGL equation in $d=2,3$ with $\alpha=0$. We also compare these numerical results with analytical expressions from Ref. [8]. We should emphasize that our methodology is also applicable to the case with $\alpha\neq 0$, as the underlying paradigm is robust, i.e., spiral defects determine the morphology in a wide range of (α,β) space.

This paper is organized as follows. Section II provides an overview of relevant analytical results. In Sec. III, we present detailed numerical results for the $d=2$ CGL equation. In Sec. IV, we present corresponding results for the $d=3$ CGL equation. Finally, Sec. V concludes this paper with a summary and discussion of the results presented in this exposition.

II. OVERVIEW OF RELEVANT ANALYTICAL RESULTS

Before presenting our numerical results, it is useful to summarize relevant analytical results for ordering dynamics in the CGL equation. Let us first discuss the case with $\alpha=\beta=0$. If the order parameter ψ is real, Eq. (1) simplifies to the time-dependent Ginzburg-Landau (TDGL) equation, which describes the ordering dynamics of a ferromagnet [6,7]. In this case, the system evolution is characterized by

the formation and growth of domains enriched in ''up'' and ''down'' spins. Domain growth is driven by a curvature-reduction mechanism, which causes the annihilation of interfacial defects. The characteristic length scale obeys the Lifshitz-Cahn-Allen (LCA) law [10], $L(t) \sim t^{1/2}$, where t is the time after the quench. An important result for ordering dynamics in the TDGL equation is due to Ohta *et al.* [11], who used an interface-dynamics approach to obtain an analytic expression for the correlation function of an ordering ferromagnet.

The LCA growth law is surprisingly robust over a wide range of physical situations described by a nonconserved order parameter [7]. When ψ is complex and $\alpha = \beta = 0$, Eq. (1) corresponds to the XY model [with $O(2)$ symmetry], and domain growth proceeds by the annihilation of vortices. Again, domain growth is described by the LCA law for $d \geqslant 2$, though there are logarithmic corrections in $d=2$, viz., $L(t) \sim (t/\ln t)^{1/2}$ [12]. The corresponding correlation function has been obtained by Puri [13].

Furthermore, Bray and Puri [14] and (independently) Toyoki [15] (BPT) have obtained the correlation function, referred to as the BPT function, for the vector TDGL equation with $O(n)$ symmetry in d dimensions when $n \leqslant d$, so that topological defects are present. The equal-time correlation function for the $O(n)$ model is defined as $C(r_{12},t) = \langle \vec{\psi}(\vec{r}_1,t) \cdot \vec{\psi}(\vec{r}_2,t) \rangle$, where $r_{12} = |\vec{r}_1 - \vec{r}_2|$, and the angular brackets refer to an averaging over independent initial conditions. The BPT function for the $O(n)$ model has the following functional form:

$$C(r_{12},t) = \frac{n\gamma}{2\pi}\left[B\left(\frac{n+1}{2},\frac{1}{2}\right)\right]^2 F\left(\frac{1}{2},\frac{1}{2};\frac{n+2}{2};\gamma^2\right), \quad (2)$$

where $B(x,y)$ is the beta function; $F(a,b;c;z)$ is the hypergeometric function [16]; and $\gamma = \exp[-r_{12}^2/(2L^2)]$, L being the average defect length scale. The appropriate domain growth law is again the LCA law, though there are logarithmic corrections when $n=d$ [7].

Next, let us consider the case with ψ complex and $\alpha, \beta \neq 0$. We will focus on the case with $\alpha = 0$, unless explicitly stated otherwise. As mentioned earlier, this case is representative of a large region of parameter space. Following the work of Hagan [17], Aranson *et al.* [18], and Chate and Manneville [19], we briefly discuss the phase diagram of the $d=2$ CGL equation with $\alpha = 0$. The limit $\beta = 0$ corresponds to the XY model, which is well understood [7,13]. Without loss of generality, we consider the case with $\beta \geqslant 0$. For $0 \leqslant \beta \leqslant \beta_1$ ($\beta_1 \simeq 1.397$ [17]), spirals (which are asymptotically plane waves) are linearly stable to fluctuations. For $\beta_1 < \beta \leqslant \beta_2$ ($\beta_2 \simeq 1.82$ [18,19]), spirals are linearly unstable to fluctuations, but the growing fluctuations are advected away, i.e., the spiral structure is globally stable. Finally, for $\beta_2 < \beta$, the spirals are globally unstable structures and cannot exist for extended times [18]. Our results correspond to the parameter regime with $\beta \leqslant \beta_2$.

We are interested in the evolution of the CGL equation from a disordered initial condition. Let us first consider the case with $d=2$. Typically, the early-time dynamics is governed by the emergence of spiral point defects. The CGL equation with $\alpha = 0$ has been studied by Hagan [17], who demonstrated that there is a family of spiral solutions as follows (in $d=2$):

$$\psi(\vec{r},t) = \rho(r) \exp[-i\beta(1-q^2)t + im\theta - i\phi(r)], \quad (3)$$

where $\vec{r} \equiv (r,\theta)$; $q \geqslant 0$ is a constant that depends on β; and m is the number of arms in the spiral. The cases with $m>0$ and $m<0$ correspond to spirals and antispirals, respectively. The limiting forms of the functions $\rho(r)$ and $\phi(r)$ are

$$\rho(r) \to (1-q^2)^{1/2}, \quad \phi'(r) \to q, \quad \text{as} \quad r \to \infty,$$

$$\rho(r) \to a r^m, \quad \phi'(r) \to r, \quad \text{as} \quad r \to 0, \quad (4)$$

where a is determined by finiteness conditions. The order-parameter amplitude $|\psi|$ saturates to its maximum value on a length scale $\xi \sim O(1)$ [9]. Hagan has presented explicit solutions for $q(\beta)$ in the cases with $m = 1,2$. We focus on the case with $m = \pm 1$, as only one-armed spirals are expected to be stable in the evolution [17]. In the limit $\beta = 0$, we have $q=0$, and the spiral solution simplifies to the vortex solution—for the $m = \pm 1$ vortex, the lines of constant phase correspond to constant θ. Spiral solutions for the general case with $\alpha, \beta \neq 0$ have been discussed by Aranson and coworkers [18,20].

The spiral defects are equivalent to vortices for lengths $L < L_c$, where $qL_c \sim O(1)$. Thus, the early-time growth is analogous to that for the XY model. At late times, the spirals experience a repulsive interaction and the system evolution statistically ''freezes'' into a state consisting of spirals and antispirals with saturation length L_s [9]. Scaling arguments suggest that $L_s \sim L_c \sim q^{-1}$.

Next, let us discuss the correlation function and the structure factor. In the present context, the correlation function is defined as

$$C(r_{12},t) = \frac{1}{V}\int d\vec{r}_1 \langle \mathrm{Re}\{\psi(\vec{r}_1,t)\psi(\vec{r}_2,t)^*\}\rangle, \quad (5)$$

where V is the system volume; and $\mathrm{Re}(z)$ refers to the real part of z. The structure factor, which is the Fourier transform of the correlation function, is defined as follows:

$$S(k,t) = \frac{1}{2}\langle (|\psi(\vec{k},t)|^2 + |\psi(-\vec{k},t)|^2)\rangle, \quad (6)$$

where $\psi(\vec{k},t)$ is the Fourier transform of the order-parameter field $\psi(\vec{r},t)$ at wave vector $\vec{k}$.

As a first approximation, we ignore spiral-spiral interactions, and assume that the CGL morphology consists of independent spirals of length L. Furthermore, we are interested in distances $r_{12} \geqslant \xi$, where ξ is the size of the spiral core. In this case, we obtain the following integral expression for the correlation function (in $d=2$) [8]:

$$C(r_{12})=\frac{(1-q^2)}{\pi}\mathrm{Re}\int_0^1 dx x\int_0^{2\pi}d\theta\frac{x+re^{i\theta}}{(x^2+r^2+2xr\cos\theta)^{1/2}}\times\exp[-iqL\{x-(x^2+r^2+2xr\cos\theta)^{1/2}\}]\times h[1-(x^2+r^2+2xr\cos\theta)^{1/2}], \quad (7)$$

where $r=r_{12}/L$; and the step function $h(y)=1(0)$ if $y\geqslant 0$ ($y<0$). Thus, the scaling form of the single-spiral correlation function is $C(r_{12})/C(0)=g(r_{12}/L,q^2L^2)$. In general, there is no scaling with the spiral size because of the additional factor qL. We recover scaling only in the limit $q=0$ ($\beta=0$), which corresponds to the case of a vortex. Essentially, spirals of different sizes are not morphologically equivalent because there is more rotation in the phase as one goes out further from the core.

The singular behavior of $C(r_{12})$ in the limit $r\to 0$ (but with $r_{12}/\xi\gg 1$) is of great interest, as it determines the large-wave-vector ($k\to\infty$) behavior of the structure factor. In Ref. [8], we undertook the necessary asymptotic analysis to obtain the following expression for the singular part as $r\to 0$:

$$C_{\mathrm{sing}}(r_{12})=\frac{1}{2}\sum_{p=0}^{\infty}\sum_{m=0}^{\infty}(-1)^{p+m}\frac{(qL)^{2(p+m)}}{(2p)!(2m)!}\times\frac{\Gamma\left(\frac{1}{2}+m\right)^2}{\Gamma\left(\frac{1}{2}-p\right)^2(m+p+1)!^2}\times(2m+1)(2p+1)r^{2(m+p+1)}\ln r. \quad (8)$$

We notice that the leading-order singularity is $C_{\mathrm{sing}}(r_{12})\simeq\frac{1}{2}r^2\ln r$, as in the case with $\beta=0$ [7]. However, there is now a sequence of subdominant singularities proportional to $(qL)^2r^4\ln r$, $(qL)^4r^6\ln r$, etc., and these become increasingly important as the length scale L increases. The subdominant terms in $C_{\mathrm{sing}}(r_{12})$ are reminiscent of the leading-order singularities in models with $O(n)$ symmetry, where n is even [7,21]. Of course, in the context of $O(n)$ models, these singularities only arise for $n\leqslant d$ as there are no topological defects unless this condition is satisfied. In the present context, all these terms are already present for $d=2$. The corresponding structure-factor tail exhibits a sequence of power-law decays, $S(k)\sim(qL)^{2(m-1)}L^d/(kL)^{d+2m}$, where m is a positive integer. Thus, though the true asymptotic behavior in $d=2$ is still the generalized Porod tail [22], $S(k)\sim L^2(kL)^{-4}$, this is seen in conjunction with other power-law decays. This point will be further elucidated when we present numerical results for the time-dependent structure factors in Secs. III and IV.

Next, we briefly consider the CGL equation in $d=3$. The relevant defects are spiral lines, which are equivalent to spirals translated in a direction perpendicular to the plane of the spiral. It is obvious that the integral expression for the correlation function remains the same, except that the distance r_{12} between points is the projected distance in the plane of the spiral. The effects of dimensionality appear explicitly in the corresponding expression for the structure factor.

In our earlier work [8], we have also examined the utility of Gaussian auxiliary field (GAF) approximations [7] to mimic multispiral morphologies. We found that the simple GAF ansatz was not reasonable, as it did not account for the order-parameter modulations at defect-defect boundaries. However, the integral expression for the correlation function obtained from a single spiral successfully describes our numerical results over extended distances. This is because the shocks between spirals effectively isolate one spiral region from the influence of other regions. As a matter of fact, the waves from other spirals decay exponentially through the shock and the phase of a point is always dominated by the nearest spiral. Therefore, we expect that the correlation function will be dominated by the single-spiral result—in accordance with our numerical results presented in Secs. III and IV.

III. NUMERICAL RESULTS IN $d=2$

We obtained numerical results in $d=2$ by implementing an isotropic Euler-discretized version of Eq. (1) on an N^2 lattice. The discretization mesh sizes were $\Delta t=0.01$ and $\Delta x=1.0$. Periodic boundary conditions were applied in both directions. The initial condition for the order-parameter field consisted of small-amplitude random fluctuations about zero, mimicking the ''high-temperature'' disordered phase of the system. In all our simulations, we set $\alpha=0$ and β was varied. Figure 1 shows the typical evolution of the system from a random initial condition for $\beta=1.25$. The black and gray regions refer to lines of constant phase, as specified in the figure caption. The asterisks denote defect centers, from where the spiral arms originate. Figure 1 demonstrates that the evolving morphology is characterized by spirals and antispirals for these parameter values.

In this section, we present numerical results for growth laws, correlation functions, and structure factors for the typical evolution morphology depicted in Fig. 1. All statistical data is obtained as an average over five independent runs for system sizes $N=1024$. We will compare our numerical results with the analytical results for a single spiral, described in Sec. II.

A. Growth laws

Figure 2 plots the square of the characteristic length scale, $L(t)^2$ vs $t/\ln t$ for five different values of β. The typical defect size is defined as $\pi L(t)^2=A/N_d(t)$, where A is the system area and $N_d(t)$ is the total number of defects at time t. In the 2D XY model (where $\beta=0$), the domain growth law is $(t/\ln t)^{1/2}$. This would correspond to a straight line in Fig. 2, though we do not present data for $\beta=0$. The data for $\beta=0.25$ are comparable to that for the XY model over the time scales of our simulation.

At early times, the spirals behave as vortices and we expect the growth law to be the same as that for the two-dimensional (2D) XY model. At later times, there is a repulsive spiral-antispiral interaction and the evolving mor-

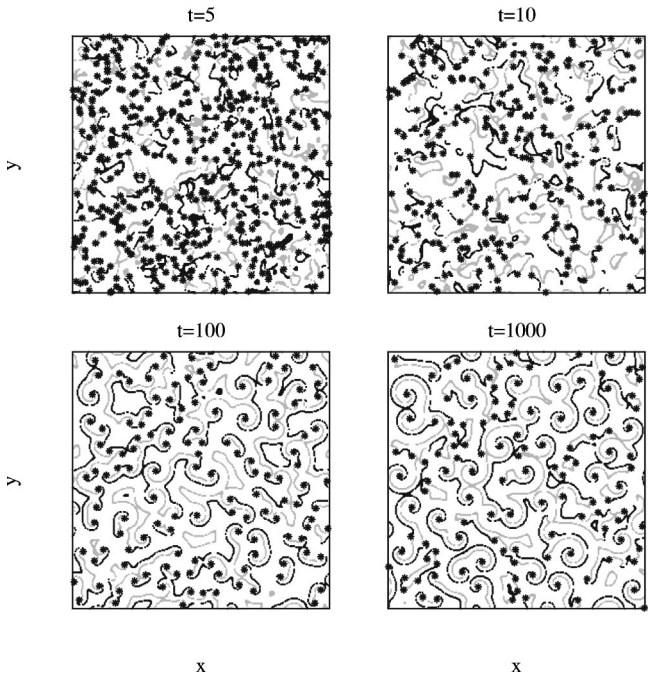

FIG. 1. Evolution from a small-amplitude random initial condition for the two-dimensional CGL equation with $\alpha=0$ and $\beta=1.25$. These pictures were obtained by implementing an isotropic Euler discretization of Eq. (1) on a square lattice of size $N^2(N=256)$, with periodic boundary conditions in both directions. The discretization mesh sizes were $\Delta t=0.01$, $\Delta x=1.0$. The snapshots, labeled by appropriate times, show lines of constant phase $\theta_\psi=\tan^{-1}(\mathrm{Im}\,\psi/\mathrm{Re}\,\psi)$, measured in radians, with the color coding: $\theta_\psi\in[1.85,2.15]$ (black); and $\theta_\psi\in[3.85,4.15]$ (gray). The asterisks denote spiral cores, defined as points around which the phase of ψ rotates by 2π.

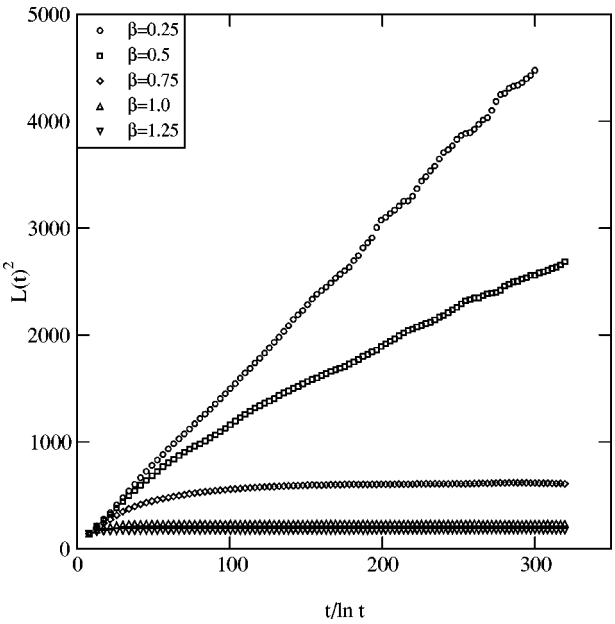

FIG. 2. Plot of $L(t)^2$ vs $t/\ln t$ for the $d=2$ CGL equation with $\alpha=0$ and $\beta=0.25,0.5,0.75,1.0,1.25$ (denoted by the specified symbols). The characteristic length scale $L(t)$ is measured directly from the evolution morphology as described in the text. For each β value, the length-scale data were obtained as an average over five independent runs for lattice sizes $N=1024$. The plot axes are chosen so that data for the XY model (not shown here) lie on a straight line.

phology ''freezes'' in a statistical sense. (The order-parameter field continues to be time dependent for all times.) As we have discussed earlier, the crossover length scale from vortex-mediated growth to spiral-mediated growth scales as $L_c\sim q^{-1}$. We determine $L_c(\beta)$ from the data sets in Fig. 2 as follows. The first three points of each data set are fitted by a straight line, and the crossover point is designated as the first point that deviates from this straight line. Figure 3 plots L_c vs q^{-1} for $\beta\in[0.5,1.0]$, and demonstrates the validity of this scaling law. (In an earlier paper [9], we have demonstrated that the saturation length $L_s\sim q^{-1}$.) As $\beta\to 0$, we expect the crossover to be proportionately delayed, as there is no freezing of domain growth in the XY model.

B. Correlation functions

We have already defined the correlation function in Sec. II. In Fig. 4, we present numerical data for the correlation functions from three different times for $\beta=1.25$. The numerical results for the correlation function were obtained by ''hardening'' the order-parameter field, i.e., setting $|\psi|=1$ before computing the correlation function or structure factor. Furthermore, the data shown in Fig. 4 are obtained by spherically averaging the corresponding vector function. The correlation-function data show a prominent dip as time in-

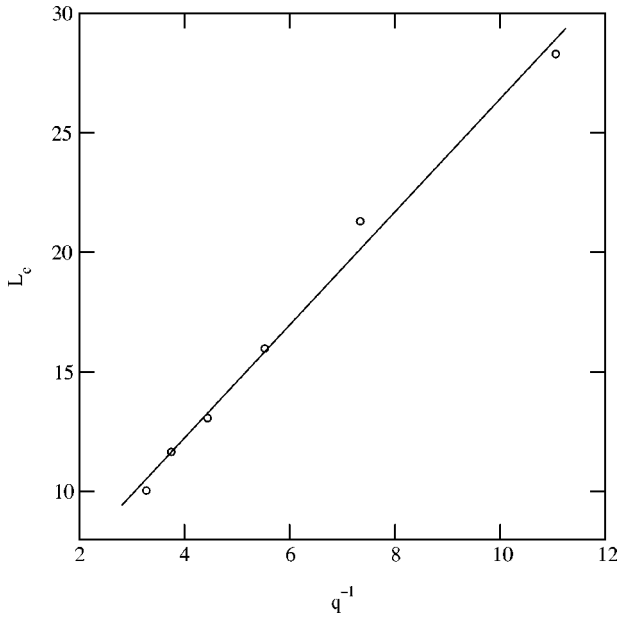

FIG. 3. Plot of crossover length scale, L_c vs $q(\beta)^{-1}$, for the the $d=2$ CGL equation with $\beta\in[0.5,1.0]$. The crossover point is located in the manner described in the text. The value of $q(\beta)$ is determined from Hagan's solution for the one-armed spiral—see Fig. 2 in Ref. [8] or Fig. 5 of Ref. [17]. The solid line refers to the best linear fit to the data.

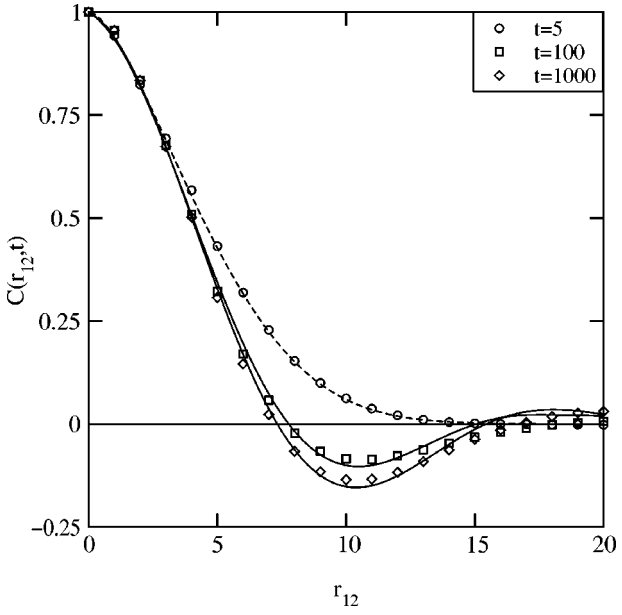

FIG. 4. Plot of correlation functions, $C(r_{12},t)$ vs r_{12}, for the $d=2$ CGL equation from three different times $t=5$, 100, and 1000 (denoted by the specified symbols). The parameter values are $\alpha=0$ and $\beta=1.25$, as in Fig. 1. The numerical data were obtained as an average over five independent runs for $N=1024$. The early-time data ($t=5$) are fitted to the BPT [14,15] function for the XY model (denoted as a dashed line), with the length scale L as a fitting parameter. The best-fit value was $L\simeq 4.40$. The later-time data ($t=100,1000$) were fitted to Eq. (7) (denoted as solid lines) with L as a fitting parameter. The best-fit values are $L\simeq 15.25$ ($t=100$); and $L\simeq 19.25$ ($t=1000$).

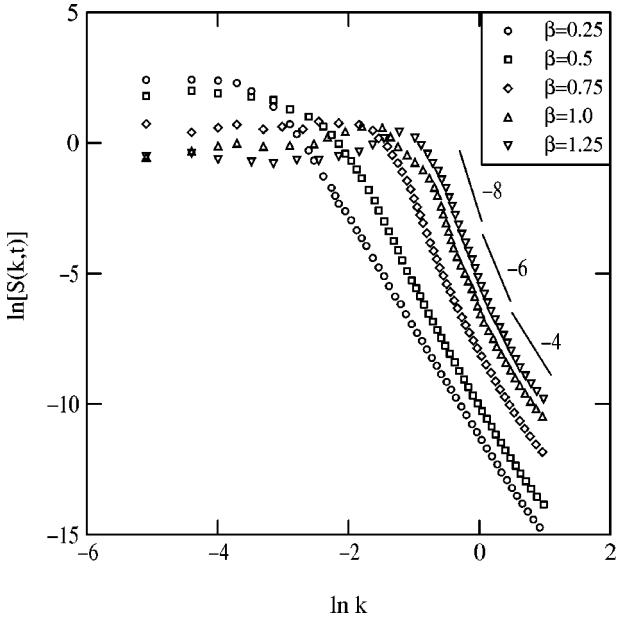

FIG. 5. Plot of structure factor, $\ln[S(k,t)]$ vs $\ln k$ for the $d=2$ CGL equation with $\alpha=0$ and $\beta=0.25,0.5,0.75,1.0,1.25$ (denoted by the specified symbols). All data sets correspond to $t=1000$. The solid lines have slopes -4, -6, and -8, as indicated. The data are normalized so that $\int_0^\infty dk S(k,t)=1$. The averaging statistics is the same as that in Fig. 4.

creases, and the spiral nature of defects become more apparent. Thus, there is no scaling of the correlation function with the defect size, in accordance with our earlier arguments.

The early-time ($t=5$) correlation function in Fig. 4 decays monotonically. It is well described by the $n=2$ BPT [14,15] function in Eq. (2) (denoted by a dashed line), which results from a GAF approximation for the XY model. This function describes a multivortex morphology, and the length scale L is chosen as a fitting parameter. The best-fit value of L is specified in the figure caption.

The correlation functions at later times ($t=100,1000$) are well described by the single-spiral correlation function (denoted by solid lines) up to the first minimum. The single-spiral function is obtained by a direct numerical integration of Eq. (7). The appropriate q value was obtained from Hagan's solution [17] for $q(\beta)$ in the case of one-armed spirals. While comparing the numerical results with the integral expression, we treated the length scale L as a fitting parameter and laterally scaled r_{12} for the analytical function to match the numerical data at $C(r_{12},t)=0.5$. In both cases ($t=100,1000$), the best-fit value is specified in the figure caption and is comparable with the average size of the defects shown in Fig. 2, which was obtained directly from the morphology. In our earlier work [9], we had compared numerical data for the correlation function for different β values with the analytical form. Though our integral expression is obtained in the context of a single-spiral morphology, the comparison is reasonable upto the first minimum. As we have discussed earlier, the correlation function is dominated by a single spiral because the shocks between spirals effectively isolate them from each other.

C. Structure factors

As discussed in Sec. II, the consequence of the singularity in the correlation function as $r\to 0$ [Eq. (8)] is a sequence of power-law decays in the large-wave-vector behavior of the structure factor, $S(k)\sim(qL)^{2(m-1)}L^d/(kL)^{d+2m}$, where $m=1,2$, etc. In $d=2$, the power-law decays are $S(k)\sim q^{2(m-1)}L^{-2}k^{-(2m+2)}$. Clearly, the asymptotic behavior is still the generalized Porod tail, $S(k)\sim k^{-4}$, as in the XY model [14], but there are also intermediate decays as k^{-6}, k^{-8}, etc. These are expected to interfere with the unambiguous observation of the generalized Porod tail.

Figure 5 plots $\ln[S(k,t)]$ vs $\ln k$ for five different values of β at $t=1000$. We have normalized the structure-factor data as $\int_0^\infty dk S(k,t)=1$. Notice that the $\vec{k}$ values in the discrete Brillouin zone are $\vec{k}=(2\pi/N\Delta x)(n_x,n_y)$, where n_x and n_y range from $-N/2$ to $(N/2)-1$. We retain data up to $k_{\max}=\pi/\sqrt{2}$. The solid lines in Fig. 5 have slopes -4, -6, and -8, corresponding to $m=1,2$, and 3, respectively. For smaller values of β (e.g., $\beta=0.25$), the contributions from the higher-order decays are small and the tail is dominated by $S(k,t)\sim k^{-4}$. However, for higher values of β, the higher-order contributions are not negligible and one sees intermediate regions with behavior $S(k,t)\sim k^{-6}$, $\sim k^{-8}$, etc. for $k<1$. Nevertheless, the tail is always seen to be parallel to the line with slope -4 for very large values of k.

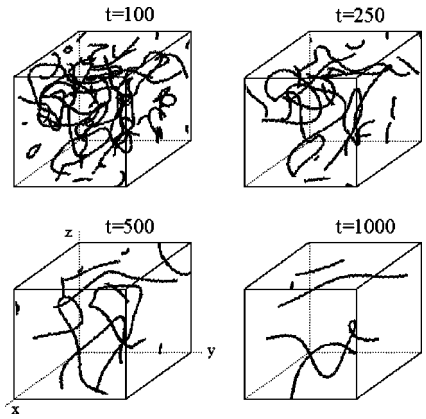

FIG. 6. Evolution of the $d=3$ CGL equation from a small-amplitude random initial condition with $\alpha=0$ and $\beta=1.25$. The pictures correspond to an N^3 lattice with $N=128$, and periodic boundary conditions are applied in all three directions. The discretization mesh sizes are $\Delta t=0.01$ and $\Delta x=1.0$. The solid lines denote regions where $|\psi|<0.5$. The snapshots are labeled by the appropriate evolution times.

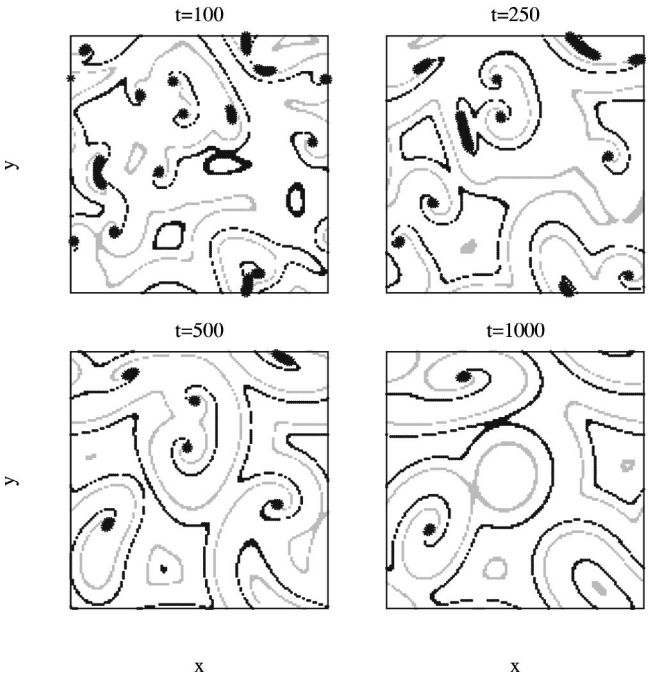

FIG. 7. Horizontal cross sections (at $z=64$) of the snapshots shown in Fig. 6. The frames show regions of constant phase $\theta_\psi=\tan^{-1}(\mathrm{Im}\,\psi/\mathrm{Re}\,\psi)$, measured in radians, with the color coding: $\theta_\psi\in[1.85,2.15]$ (black); and $\theta_\psi\in[3.85,4.15]$ (gray). The asterisks denote regions where $|\psi|<0.5$.

An alternative measure of the defect length scale is obtained by measuring the amplitude of the structure-factor tail. In each case, the results are consistent with those shown in Fig. 2, as well as the fitting length scales for the correlation function. For the sake of brevity, we do not present length-scale data obtained from the structure-factor tail.

IV. NUMERICAL RESULTS IN $d=3$

For the CGL equation in $d=3$, the defect dimensionality is 1 ($=d-n$, where n is the number of components in the order parameter). In this case, the defect cores meet and form lines, which we will refer to as spiral lines. We implemented an isotropic Euler-discretized version of the $d=3$ CGL equation on an N^3 lattice, with periodic boundary conditions. The discretization mesh sizes were $\Delta t=0.01$ and $\Delta x=1.0$. As in the $d=2$ case, the initial condition for the order-parameter field consisted of uniformly distributed small-amplitude fluctuations about zero. Again, we always set $\alpha=0$ and vary the parameter β.

Figure 6 shows the typical evolution for the $d=3$ CGL equation with $\beta=1.25$ from a disordered initial condition. The system size was $N=128$. For clarity of presentation, we only show the spiral lines, defined as regions where $|\psi|<0.5$. In Fig. 7, we show planar cross sections of the snapshots in Fig. 6. The frames of Fig. 7 are color-coded in the same manner as Fig. 1. The black and gray regions refer to lines of constant phase, as specified in the figure caption. The asterisks refer to spiral cores, defined as regions where $|\psi|<0.5$. In the early-time snapshots ($t=100,250$), we see an aggregation of spiral cores. This results from the high density of spiral lines, many of which cross the plane at points that are bunched together. This feature is absent at later times, when the density of spiral lines has thinned out appreciably.

The evolving morphology is again characterized by spirals and antispirals. At comparable values of β, freezing occurs considerably later in the $d=3$ case than in the $d=2$ case. This is because the spiral defects can relax in the perpendicular direction without experiencing a repulsive potential. In this section, we will present numerical results for the growth laws, correlation functions and structure factors for the $d=3$ CGL equation. As in the two-dimensional case, we will also compare the correlation functions and structure factors with the corresponding analytical results for a single spiral. The length-scale data is obtained as an average over five independent runs for lattice sites $N=180$. On the other hand, the correlation-function and structure-factor data are obtained from five runs for lattice sizes $N=128$.

A. Growth laws

Let us first focus on the time dependence of the characteristic defect size. Recall that the spiral line defect consists of a spiral translated in the perpendicular direction. We measure the lateral length scale by counting the number of spiral cores in all possible planar cross sections along the (x,y,z) directions. The defect length scale is then obtained as $\pi L(t)^2=A/N_d(t)$, where $A(=N^2\Delta x^2)$ is the planar area and $N_d(t)$ is the average number of defects in the plane. In general, the spiral lines are not oriented along the x, y, or z axis. Therefore, this definition underestimates the actual length scale by a constant factor, assuming that the spiral lines are randomly oriented with respect to any arbitrary plane.

For the 3D XY model, the domain growth law is $L(t)\sim t^{1/2}$. In Fig. 8, we plot $L(t)^2$ vs t for six different values of β. The growth is much faster than that in $d=2$ (Fig. 2), because of the extra degree of freedom for relaxation of the order parameter. This is apparent if one compares the evolu-

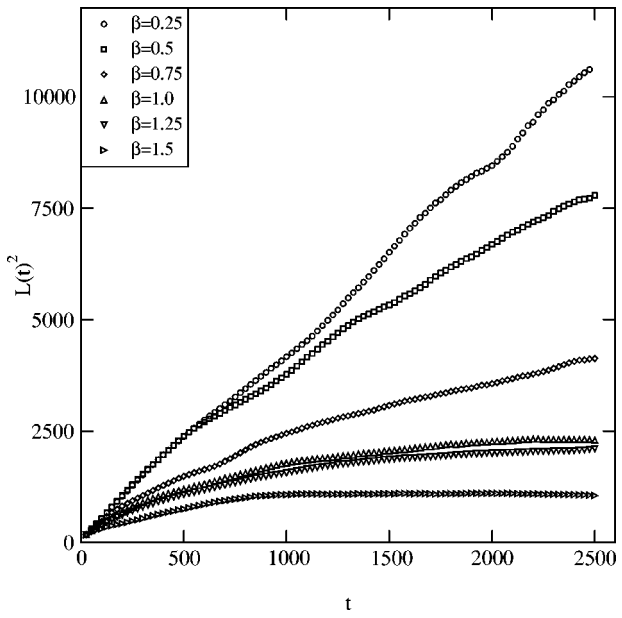

FIG. 8. Plot of $L(t)^2$ vs t for the $d=3$ CGL equation with $\alpha=0$ and $\beta=0.25,0.5,0.75,1.0,1.25,1.5$ (denoted by the specified symbols). The numerical data were obtained as described in the text by averaging over five independent runs for 180^3 lattices.

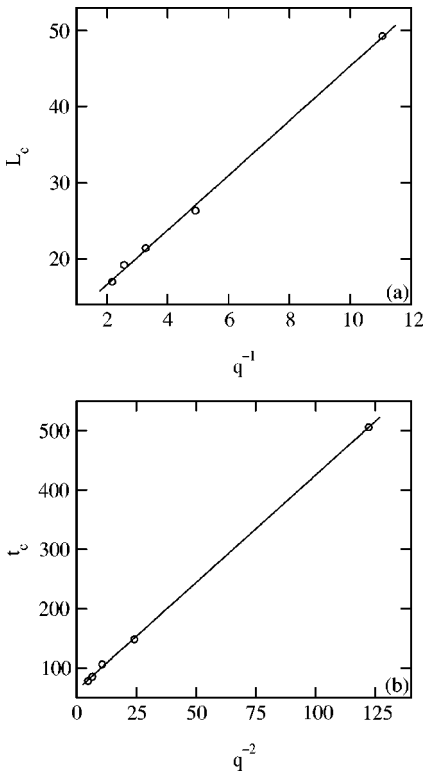

FIG. 9. (a) Dependence of crossover length scale L_c on $q(\beta)^{-1}$ for the $d=3$ CGL equation with $\beta\in[0.5,1.5]$. The crossover point is determined as described in the text. The solid line denotes the best linear fit to the data. (b) Plot of crossover time scale t_c vs $q(\beta)^{-2}$ for the data shown in (a). The solid line denotes the best linear fit to the data.

tion pictures in Figs. 1, 6, and 7. The data for $\beta=0.25$ are seen to be consistent with XY-like growth over the duration of our simulation. The data for $\beta=1.0,1.25,1.5$ show freezing, but at later times and larger length scales than the $d=2$ case (Fig. 2).

Let us investigate the crossover behavior for the length-scale data in Fig. 8. As in the $d=2$ case, we fit a straight line to the first three data points for each set. The crossover point is designated as the first point that deviates from this straight line. Figure 9(a) plots L_c vs q^{-1} for $\beta\in[0.5,1.5]$ and confirms the scaling law $L_c\sim q^{-1}$. In the early stages of growth, we have $L(t)\sim t^{1/2}$ (XY-like behavior). Thus, we expect that the crossover time $t_c\sim q^{-2}$. Figure 9(b) plots t_c vs q^{-2} and confirms this scaling behavior.

B. Correlation functions

Next, we consider the correlation-function data. As in the $d=2$ case, we spherically average the vector correlation function to obtain the scalarized function $C(r_{12},t)$. The evolving system (see Fig. 6) consists of an isotropic mixture of spiral line defects, so the spherical-averaging procedure is numerically appropriate. However, a single line defect is strongly anisotropic with perfect correlation along the line, and all decorrelations occurring in the plane of the spiral. We can still compare our numerical data with the analytical expression for a single spiral, but the quantity L will merely be treated as a fitting parameter, and is not directly identifiable as the lateral defect size.

Figure 10(a) shows the temporal evolution of the correlation function for $\beta=1.25$. The early-time data ($t=100$) decays monotonically and is well fitted by the BPT function for the XY model (denoted as a dashed line). The late-time data exhibit oscillations characteristic of spiral defects. The solid lines denote best fits to the integral expression in Eq. (7), with L as a fitting parameter. The r_{12} axis for the analytic form is also scaled so as to match the numerical data at $C(r_{12},t)=0.5$. Again, the fits are reasonably good upto the first minimum. Figure 10(b) shows the corresponding data for $\beta=1.0$.

C. Structure factors

In $d=3$, the tail of the structure factor decays as $S(k)\sim q^{2(m-1)}L^{-2}k^{-(2m+3)}$, where $m=1$, 2, etc. Figure 11 is a plot of the structure factor, $\ln[S(k,t)]$ vs $\ln k$, for six different values of β at $t=1000$. As before, the structure-factor data are normalized as $\int_0^\infty dk S(k,t)=1$. The solid lines have slopes -5, -7, and -9, corresponding to $m=1,2$, and 3, respectively. As in the $d=2$ case, one sees that for smaller values of β (e.g., $\beta=0.25$, 0.5), the contributions from higher-order decays are small and the tail is dominated by $S(k,t)\sim k^{-5}$. The higher-order contributions become more noticeable with the increase of β.

V. SUMMARY AND DISCUSSION

Let us conclude this paper with a summary and discussion of the results presented in this two-stage exposition on nonequilibrium dynamics in the complex Ginzburg-Landau (CGL) equation. In the first part of this exposition [8], we

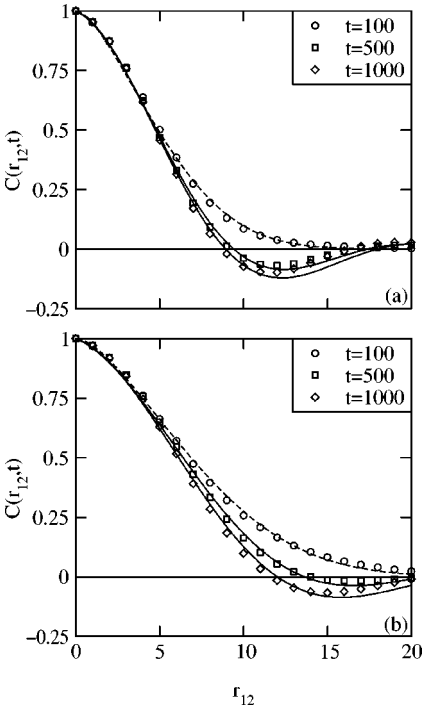

FIG. 10. Plot of correlation functions $C(r_{12},t)$ vs r_{12} for the $d=3$ CGL equation from three different times $t=100$, 500, and 1000 (denoted by the specified symbols). The numerical data were obtained by averaging over five independent runs for 128^3 lattices. (a) Data for parameter values $\alpha=0$ and $\beta=1.25$. The $t=100$ data are fit to the BPT form (dashed line) and the best-fit length scale is $L\simeq 4.9$. The data for $t=500$,1000 are fit to Eq. (7) (solid lines) and the best-fit parameter values are $L\simeq 13.6$ ($t=500$), and $L\simeq 16.2$ ($t=1000$). (b) Analogous to (a), but for $\alpha=0$ and $\beta=1.0$. The best-fit parameter values are $L\simeq 6.85$ ($t=100$); $L\simeq 13.75$ ($t=500$); $L\simeq 18.0$ ($t=1000$).

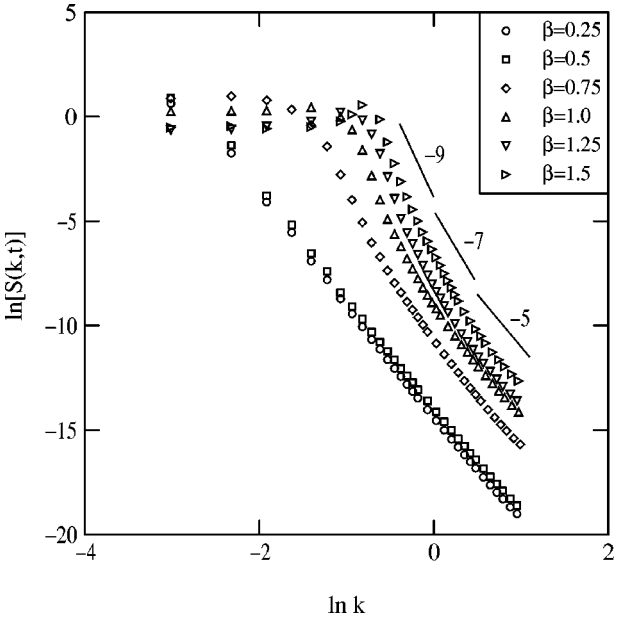

FIG. 11. Plot of $\ln[S(k,t)]$ vs $\ln k$ for the $d=3$ CGL equation with $\alpha=0$ and $\beta=0.25,0.5,0.75,1.0,1.25,1.5$ (denoted by the specified symbols). All data sets correspond to $t=1000$. The solid lines have slopes -5, -7, and -9, as indicated. The data are normalized so that $\int_0^\infty dk S(k,t)=1$. The averaging statistics is the same as that in Figure 10.

presented analytical results for the correlation function arising from a single-spiral defect. We studied this correlation function in the short-distance limit, and examined the implications of the short-distance singularities for the large-wave-vector tail of the structure factor. In particular, we found that the structure-factor tail is characterized by a generalized Porod tail, $S(k,t)\sim k^{-(d+2)}$ for large k, as in the XY model. However, there are also subleading decays, $S(k,t)\sim k^{-(d+2m)}$ with $m>1$, which would interfere with the unambiguous observation of the generalized Porod tail.

This paper constitutes the second and final part of this exposition. Here, we have presented detailed numerical results for domain growth laws; correlation functions; and structure factors for phase ordering dynamics in the CGL equation in $d=2,3$. We find that the spirals behave as vortices at early times [$L(t)<L_c$, where $qL_c\sim O(1)$], i.e., the early-time behavior is analogous to that for the XY model. At later times, the spiral nature of the defects plays an important role in two respects. First, there is a repulsive spiral-antispiral interaction that leads to the statistical freezing of domain growth. The saturation length scale depends upon β as $L_s\sim q(\beta)^{-1}$ [9]. Second, the correlation function exhibits a crossover from a monotonically decaying XY-like form to an oscillatory form, which does not scale with the defect size.

In this paper, we have also presented numerical results for the structure factor. Our results elucidate the nature of the structure-factor tail—the asymptotic behavior is the generalized Porod law, but this appears in conjunction with a sequence of higher-order power-law decays. The subdominant behavior is accentuated at larger values of β.

Finally, we would like to again stress the general nature of our results. In this exposition, we have confined ourselves to presenting analytical and numerical results for $\alpha=0$ and $\beta\neq 0$. However, the underlying paradigm remains the same in an extended region of parameter space, viz., spirals govern the temporal evolution and spatial morphology of the CGL equation for a wide range of (α,β) values. The results of this exposition apply directly in that case also, with appropriate modifications in the functional form of the spiral solution [18,20].

ACKNOWLEDGMENTS

The authors are grateful to M.C. Cross for a fruitful collaboration in the first stage of this exposition. S.P. is grateful to A.J. Bray and H. Chate for useful discussions. S.K.D. thanks D. Srivastava for helpful inputs. S.K.D. is also grateful to the University Grants Commission, India, for financial support.

[1] For example, see S.C. Müller, T. Plesser, and B. Hess, Physica D **24**, 71 (1987); G.S. Skinner and H.L. Swinney, *ibid.* **48**, 1 (1991).
[2] R.W. Walden, P. Kolodner, A. Passner, and C.M. Surko, Phys. Rev. Lett. **55**, 496 (1985); E. Moses and V. Steinberg, Phys. Rev. A **34**, 693 (1986).
[3] F.T. Arecchi, G. Giacomelli, P.L. Ramazza, and S. Residori, Phys. Rev. Lett. **65**, 2531 (1990); **67**, 3749 (1991).
[4] M.C. Cross and P.C. Hohenberg, Rev. Mod. Phys. **65**, 851 (1993).
[5] A.C. Newell, *Solitons in Mathematics and Physics*, CBMS Vol. 48 (SIAM Press, Philadelphia, 1983).
[6] K. Binder, in *Phase Transformations of Materials*, edited by R.W. Cahn, P. Haasen, and E.J. Kramer, Materials Science and Technology Vol. 5 (VCH, Weinheim, 1991), p. 405.
[7] A.J. Bray, Adv. Phys. **43**, 357 (1994).
[8] S.K. Das, S. Puri, and M.C. Cross, Phys. Rev. E **64**, 046206 (2001).
[9] S. Puri, S.K. Das, and M.C. Cross, Phys. Rev. E **64**, 056140 (2001).
[10] I.M. Lifshitz, Sov. Phys. JETP **15**, 939 (1962); S.M. Allen and J.W. Cahn, Acta Metall. **27**, 1085 (1979).
[11] T. Ohta, D. Jasnow, and K. Kawasaki, Phys. Rev. Lett. **49**, 1223 (1982).
[12] A.N. Pargellis, P. Finn, J.W. Goodby, P. Panizza, B. Yurke, and P.E. Cladis, Phys. Rev. A **46**, 7765 (1992); B. Yurke, A.N. Pargellis, T. Kovacs, and D.A. Huse, Phys. Rev. E **47**, 1525 (1993).
[13] S. Puri, Phys. Lett. A **164**, 211 (1992); see also S. Puri and C. Roland, *ibid.* **151**, 500 (1990).
[14] A.J. Bray and S. Puri, Phys. Rev. Lett. **67**, 2670 (1991).
[15] H. Toyoki, Phys. Rev. B **45**, 1965 (1992).
[16] I.S. Gradshteyn and I.M. Ryzhik, *Table of Integrals, Series, and Products*, edited by A. Jeffrey (Academic Press, London, 1994).
[17] P.S. Hagan, SIAM (Soc. Ind. Appl. Math.) J. Appl. Math. **42**, 762 (1982).
[18] I.S. Aranson, L.B. Aranson, L. Kramer, and A. Weber, Phys. Rev. A **46**, R2992 (1992); A. Weber, L. Kramer, I.S. Aranson, and L.B. Aranson, Physica D **61**, 279 (1992).
[19] For example, see H. Chate, Nonlinearity **7**, 185 (1994) for the $d=1$ CGL equation; H. Chate and P. Manneville, Physica A **224**, 348 (1996) for the $d=2$ CGL equation.
[20] I.S. Aranson, L. Kramer, and A. Weber, Phys. Rev. E **47**, 3231 (1993).
[21] A.J. Bray and K. Humayun, Phys. Rev. E **47**, R9 (1993).
[22] G. Porod, in *Small-Angle X-Ray Scattering*, edited by O. Glatter and O. Kratky (Academic Press, New York, 1982); Y. Oono and S. Puri, Mod. Phys. Lett. B **2**, 861 (1988).